Comprehensive mechanical and tribological characterization of metal-polymer PTFE+Pb/Bronze coating by in-situ electrical contact resistance measurement augmented

Tribology International 193 (2024) 109397

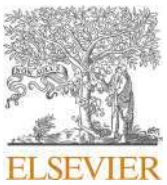

Contents lists available at ScienceDirect

Tribology International

journal homepage: www.elsevier.com/locate/triboint

Comprehensive mechanical and tribological characterization of metal-polymer PTFE+Pb/Bronze coating by in-situ electrical contact resistance measurement augmented tribo-mechanical tests

Giacomo Maculotti [a,*], Edoardo Goti [b], Gianfranco Genta [a], Luigi Mazza [b], Maurizio Galetto [a]

[a] Department of Management and Production Engineering, Politecnico di Torino, Corso Duca degli Abruzzi 24, 10129 Turin, Italy
[b] Department of Mechanical and Aerospace Engineering, Politecnico di Torino, Corso Duca degli Abruzzi 24, 10129 Turin, Italy

ARTICLE INFO

Keywords:
Self-lubricating coating
Nanoindentation
Wear
Friction

ABSTRACT

This work thoroughly mechanically characterizes the DU® metal-polymer coating from GGB Bearing Technology by augmented multi-scale Instrumented Indentation Test (IIT). Nano-IIT will evaluate the uniformity of the Pb particles dispersion in the outermost layer. Dynamic nano-IIT will investigate the damping properties of the material as a function of load frequency. Micro-IIT will tackle the layer thickness evaluation and the gradient of mechanical properties through the layers by continuous multi-cycle indentations. Data augmentation provided by synchronous electric contact resistance (ECR) measurements will support the identification of the layer transitions. The coefficient of friction and the wear coefficient will also be obtained by linear reciprocating pin-on-disc testing with focus on the specific application to guide bushings for linear pneumatic actuators.

1. Introduction

High-lubricity metal-polymer PTFE-based coating materials were developed as an alternative to traditional low-friction metallic materials, like bronze or lead, for sliding bearing elements. This special class of metal-polymer coatings relies on the exceptionally high tribological performance of PTFE, which guarantees a friction coefficient lower than traditional materials. Since their introduction, metal-polymer PTFE-based coatings have spread throughout the market and covered several applications in the field of power transmission and automation, where soft driving of sliding and rotating mechanical components is required under moderate load with very low frictional losses. Recently, these materials have also been introduced in bio-mechanical applications and bio-engineering systems. The peculiar self-lubricating behaviour of PTFE bears contact load and sustains interfacial sliding motion even without the addition of any lubricating matter, like oils or greases. This is a strategic feature for very sensitive applications in controlled environments, e.g. for surgery machines and other medical applications, and in the food industry, where bleeding of fat contaminants must be absolutely avoided [1].

The application of these coatings is also expedient where the guiding elements need to withstand the chemical action of corrosive environments or highly reactive substances like strong acids and bases. In fact, PTFE is one of the most resistant and inert substances to chemical etching because of its extremely high bonding energy, and contact with aggressive substances like acetone, chloroform, nitric acid or sulfuric acid is possible for extremely long periods without decomposition of its chemical structure.

PTFE-based composites usually exhibit a low coefficient of friction (CoF) values under a wide range of load and speed, both against themselves and metals [2]. This peculiarity is related to its very low surface energy, which nullifies the adhesion forces sticking effects with any other solid material in contact with it. The surface energy of PTFE is as low as 0.018 J/m^2 [3], i.e. hundred times lower than a metal surface. Furthermore, the formation of a transferred layer made of macromolecules stretched in the direction of sliding contributes to friction reduction [4]. In the case of PTFE against steel, the transfer is quite easy since fluorine molecular polar heads interact with the metallic material. However, PTFE at room temperature reacts to contacting bodies, disclosing a relatively soft viscoelastic behaviour due to its partially crystalline polymeric structure with low glass transition temperature (T_g) values. Therefore, the characteristic wear rate as pure material is rather high. When slid against harder bodies, pure PTFE suffers both plastic flow at the contact region and deep abrasion [5] that produce wear rates in the order of $(4-7) \times 10^{-4}$ mm^3/mN against steel [6,7]. Consequently, many strategies have been recently introduced to develop

* Corresponding author.
E-mail address: giacomo.maculotti@polito.it (G. Maculotti).

https://doi.org/10.1016/j.triboint.2024.109397
Received 27 March 2023; Accepted 4 February 2024
Available online 8 February 2024

PTFE-based composites to increase the mechanical strength and wear resistance. PTFE may be found in the scientific literature reinforced by the addition of suitable particles fillers into the polymeric matrix, e.g. graphite [8] and carbon nanoparticles [9], copper [10], bronze particles [11] or glass fibers [12]. Khedkar et al. [13] showed that fillers are able to increase hardness and wear resistance values with limited impact on the friction coefficient, which remains as low as for pure PTFE. Alternatively, it may be co-deposited inside metal coatings, like Ni-coatings, through sintering-like processes [4].

For the specific application to plain bearings and bushings, metal-polymer composite coatings with reinforcing low-friction metal structure proved to be the most effective solution. This technology was first introduced in 1956 by GGB Inc [14] and exploits the symbiotic tribological mechanism between PTFE and a low friction tin-bronze porous structure. This solution optimally combines the mechanical properties of tin-bronze, which bears part of the contact load preventing PTFE from wearing out too quickly, and the self-lubricating properties of the polytetrafluorethylene. Metal-polymer coatings are usually manufactured as strips composed of a steel sheet reinforcement on which the porous bronze matrix is sintered with a thickness of (0.2–0.4) mm. Through a special rolling operation, a PTFE-based polymer is impregnated in the open porosity of the sintered layer and forms an additional sliding layer with a thickness on top. PTFE may be enriched with a variety of additives, e.g. lead [14], graphite [15], molybdenum disulfide [16], depending on the manufacturer. These composite materials have a typical coefficient of friction that ranges from 0.4 to 0.22, and high mechanical strength, up to 20 kN/cm^2. They can operate at temperatures from − 200 °C up to 280 °C with extraordinary chemical stability and good thermal conductivity, and they can absorb shocks and vibration of the contact interface [17].

Among the others, one application of interest for this kind of composite coatings is the manufacturing of guide bushings for linear pneumatic actuators. Pneumatic cylinders are one of the most common actuators used in the industrial field due to their low cost, high cleanliness and power-to-weight ratio. A fundamental aspect that has recently allowed them to expand their field of applications is their integration into servo systems for highly automated Industry 4.0 production lines. Currently, a major limitation in this regard is the wear-out of the guiding elements, which causes the rapid deterioration of the sealing elements and, consequently, the out-of-service condition of the whole system. This applies especially when radial loads act on the piston rod, for instance, in cylinders that are required to handle or convey materials. The guide bushings installed in the front head of the actuator is the component subjected to the greater reaction force in the presence of external forces, and the metal-polymer coating may wear out quickly as a consequence.

The literature reports some research works where component testing was carried out to investigate the wear process of the guide bushings of pneumatic actuators [18–20]. Numerical simulations [21] were also performed to assess how the design of the bushing seat affects the stress distribution at the bushing-rod interface and the resulting wear. However, the heterogeneous composition and the multiphasic non-isotropic structure of the metal-polymer coatings is a challenging aspect to be dealt with for accurate numerical simulation of the contact problem. A gradient of mechanical properties is expected along the thickness of metal-polymer coatings, and some inhomogeneity in the mechanical behaviour is to be accounted for due to the inherent manufacturing process.

Despite the wide application of this class of coatings, a thorough characterization of the mechanical and tribological behaviour of PTFE-based metal-polymer composite coatings with reinforcing low-friction metal structure is still missing. To the best of the authors' knowledge, the available literature on this topic is represented by a few research papers, which only presented application-oriented tribological results. Fote et al. [22] successfully applied the adhesion friction theory to identify the relationship between CoF and temperature in vacuum ball-on-flat tests with a commercial DU® metal-polymer coating against steel. Tevruz [23] investigated the tribological behaviour of 60% bronze-filled PTFE bearings with a dedicated journal friction apparatus. Gungor et al. [24] investigated the wear behaviour of self-manufactured composite plain bearings made of sintered bronze filled with graphite-additive PTFE against a rotating steel shaft in dry conditions. Zhang et al. [25] performed very similar tests with a similar material exploring the effect of different lubricant media on friction and wear, including gasoline, engine lubricant oil, glycerol and triethanolamine. Ku et al. [26] compared a coating made of a sintered porous bronze with a PTFE overlay with a sintered coating of Al-6Sn-6Si under the typical tribological conditions of plain bearing supporting the shaft of gas compressor. Kim et al. [27] presented a study on the effect of burnishing on the life and linear wear of an modified PTFE+CaF2/Sintered bronze plain bearings for application in compressors with controlled clearance, and compared their performance to those of commercial PTFE+Pb/-Sintered bronze coatings. Goti et al. [28] recently investigated the tribological behaviour of the commercial DU® metal-polymer coating used for guide bushing of pneumatic actuators through pin-on-disk tests.

The goal of this research work is to contribute to a thorough characterization of the surface mechanical properties of the PTFE/Sintered Bronze composite coatings for plain bearings and bushings. Thus far unreported mechanical characterization will be achieved by Instrumented Indentation Tests (IIT) and complemented with tribological experiments. The mechanical characterization will be innovatively augmented with in-situ electric contact resistance measurement (ECR) to correlate electromechanical response to material structure and to propose non-destructive investigation methods. The characterization will be performed with a multi-scale approach, also tackling elastic and viscoelastic properties of the material.

2. Materials and methods

The material considered in this research work is a PTFE+Pb/Bronze composite coating manufactured by GGB Bearing Technology Inc (Thorofare, New Jersey, USA) under the trademark DU®. According to the datasheet, the nominal composition of the coating consists of steel lamina as backing coated with a low-friction lining made up of two superimposed layers. The innermost layer is a porous bronze sintered structure impregnated with a polymer compound of PTFE filled with Pb; the nominal thickness is about 280 μm. The outermost sliding layer consists of a 22 μm thick lining made of the same PTFE+Pb compound. The embedded bronze porous structure strengthens the metal-polymer coating, while the PTFE-based polymer composite provides self-lubricating properties. During the running-in period, part of the PTFE-based material is transferred to the opposite surfaces, forming a protective third layer that insulates the metallic centrode from direct contact with the coating.

2.1. Microscopy inspection

Topographical characterization was carried out with a coherence scanning interferometer (CSI) Zygo NewView9000 with a Michelson objective (magnification 5.5 ×, numerical aperture 0.15, field of view of (1.56 ×1.56) mm with squared pixels of 1.56 μm side). Ten locations on the top surface of the outermost layer (PTFE+Pb) were considered. F-operator to perform plane correction by least-square estimation and a Gaussian L-filter with a nesting index of 0.8 mm were applied [29–31]. The resulting scale limited (SL)-surface parameters are reported according to standard practice [29,32].

Additionally, the coating cross-section was inspected under the optical microscope (Leica Z16 APOA, Germany), as shown in Fig. 1. In order to accurately measure the thickness of each layer of the coating, the sample was mounted with a cold curing resin and cut perpendicularly to the surface with a high-speed precision cutting disc 0.1 mm thick. The rigid mounting resin protected the soft outermost layer during

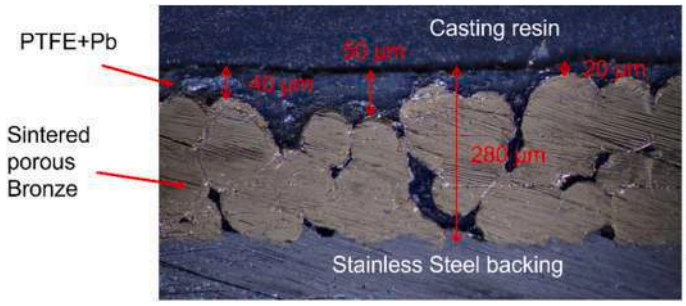

Layer	Nominal thickness / µm	Measured thickness / µm
Steel backing	1197	-
Sintered porous Bronze	278	280±10
PTFE+Pb	22	50±20

Fig. 1. Cross-section view of the DU® coating from GGB Inc with measurement of the characteristic thickness of the innermost and outermost layer.

the cutting operations preventing plastic deformation from occurring. The formation of chips from plastic flow at the trailing edge of the cutting disc would have indeed distorted the measurement of the projected thickness of the layer. Thickness measurements were performed considering 5 different positions, with a field of view of (0.5 ×0.82) mm, and taking 25 depths measurements from the casting resin edge to the sintered porous bronze, uniformly spaced. Results are reported in Fig. 1 in terms of average and expanded uncertainty, estimated from the sample standard deviation with a coverage factor $k = 2$.

2.2. Instrumented indentation test for mechanical characterization

Instrumented Indentation Test (IIT) is a depth-sensing nonconventional hardness measurement technique allowing the characterization of materials in terms of indentation hardness H_{IT}, Young modulus estimate, i.e. the indentation modulus E_{IT}, creep and relaxation from macro to nano scale. IIT applies a loading-holding-unloading force-controlled cycle with an indenter of known and calibrated shape to a test specimen [33]. During the indentation cycle, the applied force F and indenter penetration depth h in the material are measured, and the analysis of the measured quantities allows characterization relying on fundamental equations which are standardized [34–36]. IIT allows characterizing composite materials [37,38], coating and surface treatments [39], distinguishing and quantitatively characterizing different phases and structure variations of materials. The calibration of the area shape function, i.e. a relationship between h and the projected contact area A_p allows resolving properties at the nanoscale [33,40,41]. The indentation platform requires calibration of the force and displacement scales and of the frame compliance and geometry of the indenter to ensure traceability and correct systematic errors, mainly due to elastic displacement and geometric imperfection of the indenter [33,40–42].

IIT data augmentation by in-situ electrical contact resistance (ECR) allows estimating electromechanical properties, identifying differences in the microstructure due to a different electrical response [43], and quantifying critical stress states inducing phase transformation in the material [44]. ECR relies on a doped-diamond conductive indenter and applies a controlled current at the contact between the indenter and the test sample surface. While the indentation cycle is performed, the voltage is measured, and changes in the contact resistance are appreciated, see Fig. 2, allowing electromechanical characterization [45,46].

In this work, multi-scale characterization is performed by a state-of-the-art indentation platform Anton Paar STeP6, in-house prototyped to support ECR measurements, see Fig. 3. The resistance measurement includes contribution of the electrical connectors, the cables and the indenter, which are constant during the tests [45,46]. Variation of the measured resistance is analysed and focused on, to appreciate the change in the material, neglecting the resistance quantification per each particular material.

A modified version of the technique consists in applying consecutively at the same location with increasing maximum test force. This approach is indicated as continuous multi cycle (CMC) [35] and allows characterizing material properties in depth. In fact, it achieves a characterization of the mechanical properties as a function of the (increasing) maximum penetration depth $h_{c,max}$, because each successive unloading which results in a mechanical characterization value, e.g. E_{IT}, H_{IT}, can be related to a maximum penetration depth.

More recently, dynamic indentations have been introduced. These consist of superimposing a sinusoidal trend to a conventional loading-holding-unloading cycle. Such experimental setup allows evaluating viscoelastic properties of the material in terms of the loss modulus E'' and the storage modulus E'. These represent the complex and real part of the indentation modulus, i.e. $E_{IT} = E' + E''i$, whose evaluation is essential to provide thorough evaluation of polymeric materials also apt for damping. The real part E' represents the storage modulus, the complex part, i.e., E'', the loss modulus. In particular, the system is modelled as a parallel connection of a spring S_d and a dashpot D_d, connected in parallel to a simple harmonic oscillator modelling the system, with mass m, stiffness k_s and damping D_s which require calibration, see Fig. 4, and oscillating with a period ω. Once the transfer function between the applied load F_{d0} and the resulting displacement h_{d0} is calibrated, the

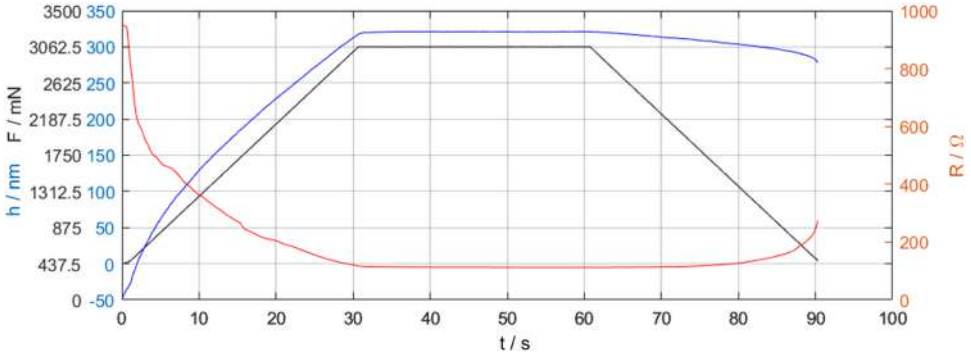

Fig. 2. Force, penetration depth and electrical resistance as a function of test time. Notice the continuous decrease of the measured resistance for increasing contact, and when a significant unloading has taken place (t > 80 s) an increase of the resistance. Sample indentation on a uniform material.

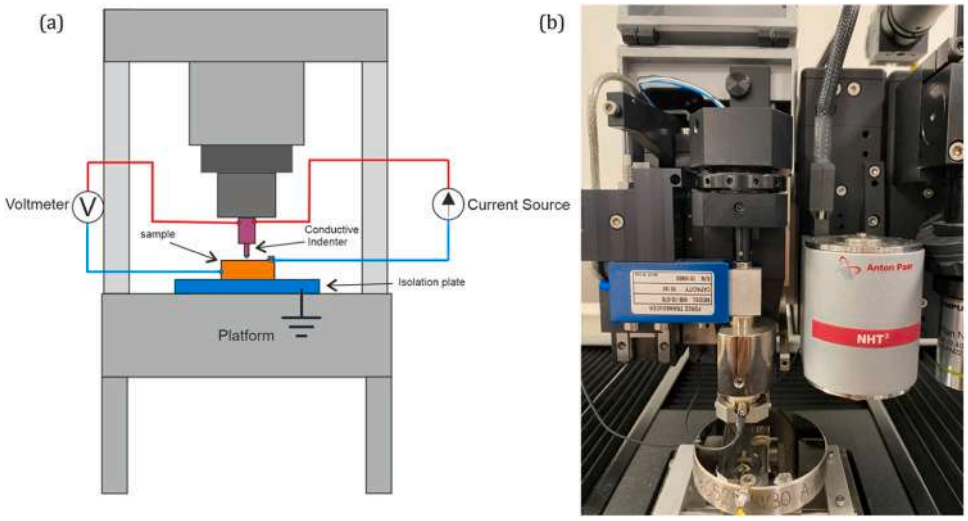

Fig. 3. (a) Scheme of the ECR setup. (b) Experimental setup with state-of-the-art Anton Paar MCT3 and NHT3 prototyped to support the ECR data augmentation in the Mind4Lab of DIGEP-PoliTO.

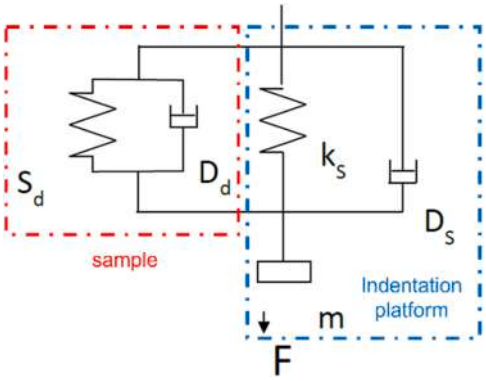

Fig. 4. Dynamic model of the machine (blue) and the sample (red).

phase difference Δφ is known, material properties can be evaluated as in Eq. (1) [47,48].

$$E' = \frac{\sqrt{\pi}}{2\sqrt{A_p}} S_d \tag{1.1}$$

$$E'' = \frac{\sqrt{\pi}}{2\sqrt{A_p}} \omega D_d \tag{1.2}$$

$$S_d = \left|\frac{F_{d0}}{h_{d0}}\right| \cos(\Delta\varphi) - k_s + m\omega^2 \tag{1.3}$$

$$\omega D_d = \left|\frac{F_{d0}}{h_{d0}}\right| \sin(\Delta\varphi) - \omega D_s \tag{1.4}$$

2.2.1. PTFE+Pb characterisation

The mechanical characterization of the outermost coating layer of PTFE+Pb was performed with a piezoelectric measurement head NHT^3. Quasistatic indentation cycles with loading and unloading of 30 s and a holding of 10 s were performed. Two indentation maps were performed on the PTFE+Pb coating at 7 mN and 10 mN. Each map consisted of an equally spaced grid of 7 × 7 indention with a step of 90 μm. Characterization of elastic mechanical properties in terms of H_{IT} and E_{IT} is considered to investigate the homogeneity of the outermost coating layer.

Additionally, viscoelastic properties of the PTFE+Pb outermost layer are characterized by dynamic indentation. A set of 15 indentions with a step of 90 μm was performed with a maximum load of 10 mN. Also, a full factorial design was deployed to evaluate the loading frequency and the material effect on the mechanical properties. Different oscillation frequencies superimposed on the holding part of the indentation cycle were considered, i.e. (1, 2, 3, 5) Hz. The considered frequency range is relevant for the main application of the coating for bushing of linear pneumatic actuators. Oscillation amplitude was kept at 5% of the maximum load [47,49]. Additionally, the material response was investigated considering the PTFE+Pb and a bulk PTFE. ANOVA will be exploited to assess the influence of sample material and loading frequency.

2.2.2. Micro-scale characterization

IIT in the micro range is exploited to characterize the material's mechanical properties as a function of the distance from the surface by applying CMC indentation. This methodology allows obtaining results without cross-sectioning the sample. Micro-IIT aims at characterizing both layers of the material, i.e. the PTFE+Pb and the porous sintered Bronze. Micro-IIT data are augmented with ECR to correlate the mechanical results with the composition of the multi-layer coating under investigation, considering that the PTFE+Pb is expected to be significantly more insulating than the sintered bronze. Micro-IIT CMC indentations were performed with a state-of-the-art Anton Paar MCT^3, considering 36 indentations. Each CMC consisted of 15 cycles with a quadratically increasing maximum load from 0.5 N to 30 N, with a loading, holding and unloading each lasting 30 s. Additionally, a second set of 18 CMC with the same parameters but ranging from 0.01 N to 0.5 N were performed with the NHT^3 head to gather additional data at shallow depths.

Regression of the mechanical properties as a function of the penetration depth will be investigated to determine relationship useful for modelling purposes of the material applications (as discussed in the introduction) in future work by numerical approaches, e.g. FEM.

ECR was enabled by applying a controlled current source at 10 mA and limiting the voltage to 6 V. This setup allows safe application of ECR to avoid sparks and electrical arcs formation but limits the maximum measured resistance to a saturation value of 600 Ω.

2.3. Tribological characterization

Experimental data from rotary pin-on-disk tests against a 6 mm steel sphere obtained by the authors in a previous investigation [28]

overestimated the typical wear rate of guide bushings observed during accelerated endurance tests carried out with a dedicated test rig for linear pneumatic actuators [19]. Therefore, for this paper, the pin-on-disk tests were carried out in linear reciprocating sliding motion against a flat steel pin 2.3 mm in diameter as a counterpart. The average roughness of the pin was Ra (0.677 ± 0.088) μm. This testing condition was preferred to reproduce better the contact state between the guide bushing of a pneumatic cylinder and the piston rod because some degree of contact conformity is expected due to geometry and local deformations. The average contact pressure on the flat pin was 12 MPa which corresponds to the maximum pressure on the bushing according to the available numerical model by Ambu et al. [19]. A TRB tribometer by Anton Paar was used. The applied load was 50 N for all the tribological tests, the stroke length was 25 mm and the maximum sliding speed was 0.25 m/s. The value of the maximum speed was set equal to the typical rod extension speed in pneumatic cylinders. The samples for the experimental tests were cut out of a GGB DU® strip used to manufacture the bushings of the pneumatic cylinders via deep-drawing.

The total sliding distance was 1900 m. The duration of the tests was chosen so that the pin could reach through the innermost layer of the coating, where the sintered bronze structure dominates the behaviour of the coating. Additional tests were carried out over a set of a shorter sliding distances, i.e. 130 m, 290 m and 1100 m, to track the evolution of the wear volume. Four tests were performed for each sliding distance to cater for measurement reproducibility.

During the tribological tests, tribological data were augmented by an in-house prototyped system for in-situ electric contact resistance (ECR) measurements to monitor the state of the interface. The 2-wire resistance measurement was performed by means of a National Instruments VirtualBench® VB-8012. The Digital MultiMeter (DMM) of the acquisition system was piloted with a LabVIEW routine developed for the purpose with an acquisition rate of 4 Hz. The schematic of the ECR measurement setup is provided in Fig. 5. The resistance measurement includes contribution of the electrical connectors, the cables and the soldered junctions, which are constant during the tests [45,46]. Variation of the measured resistance is analysed as the evidence of changes occurring at the interface, while the quantification of the interface resistance per se was not of interest.

2.3.1. Wear volume characterization

Volume is characterized in terms of the wear volume V_w, i.e., the amount of material removed, and galling volume V_g, i.e., the amount of material plastically displaced [50]. The effective damage is estimated as in Eq. (2), considering the coating functionality [51].

$$V_{eff} = V_w - V_g \tag{2}$$

The Archard wear rates were estimated based on the values of V_{eff}, and considering in first approximation the increase in wear volume to be piecewise linear. Measurements of the damaged volumes are performed by surface topography measurements carried out before and after the tribological test to remove the effect of surface topography [52,53]. Measurements were performed by a coherence scanning interferometer (CSI) Zygo NewView9000 with a Michelson objective (magnification 5.5 ×, numerical aperture 0.15, field of view of (1.56 ×1.56) mm with squared pixels of 1.56 μm side). Measurements were aligned by machine vision algorithms [52], and subtracted pixel-by-pixel to evaluate the effect of the wear. On the surface resulting from the difference, V_w and V_g are evaluated as volume topographical parameters, i.e., the void volume and the material volume with the inverse material ratio set at the undeformed reference surface [52,53]. Uncertainty was propagated considering the metrological characteristics of the surface topography measuring instrument [53,54]. Table 1

3. RESULTS AND DISCUSSION

3.1. Topographical characterization

Fig. 6 shows a representative measured surface topography. As it can be appreciated, no significative planarity deviation can be appreciated. Table 2 reports the main areal surface topographical parameters. Height parameters (Sa, Sq, SSk, Sku, Sp, Sz) describe a surface dominated by pits and scratches (Ssk < 0) mostly due to sharp and isolated features (Sku >> 3). In terms of magnitudes of peaks and valleys, the height range is evenly split (Sp~Sz/2) [29]. Qualitatively and in agreement with height parameters, isolated dales are present, mostly corresponding to surfacing bronze particle, i.e. to region where the outermost layer of PTFE+Pb was poorly deposited. Spatial parameters (Sal, Str) inform about autocorrelation and anisotropy. The surface is dominated by random and poorly autocorrelated topographical elements, Sal indicates an almost immediate decay of the autocorrelation at 41.65 μm, which is also fairly isotropic and symmetric at Str= 82.2% [55]. The hybrid spatial parameter Sdq is the root mean square gradient of the surface height and indicates a surface without significant and abrupt changes, thus providing further quantitative information on the severity of the surface spikiness and complexity [31].

3.2. Mechanical characterization

3.2.1. PTFE+Pb characterisation

Results of the surface mapping in terms of indentation modulus and indentation hardness are shown in Fig. 7. Maximum penetration depth resulted in average (3.285 ± 0.486) μm (see Fig. 8(a)), slightly in excess to the standard conservative prescription of the 10% of the nominal PTFE+Pb layer thickness (see Fig. 1) [56]. It is worth noting that such a prescription is satisfied well when considering the measured thickness (see Fig. 1). Both the mechanical characteristics did not show significant departures from normal distribution when tested with an Anderson-Darling test. However, the greater robustness of the E_{IT} allows identifying outliers in the surface, as it is apparent in Fig. 7. Such outliers can be related to surfacing bronze particles inherent in the material structure (see Fig. 1). Hypothesis testing (*t*-test) at a 95% confidence level could not highlight any systematic differences in the mechanical

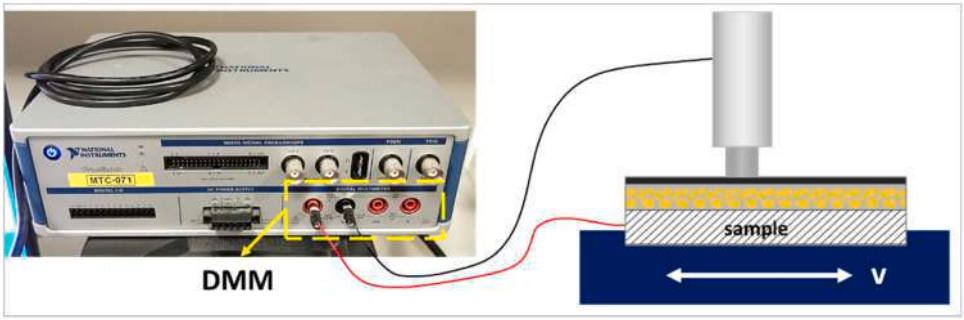

Fig. 5. Setup of the 2-wire ECR measuring system for tribological tests.

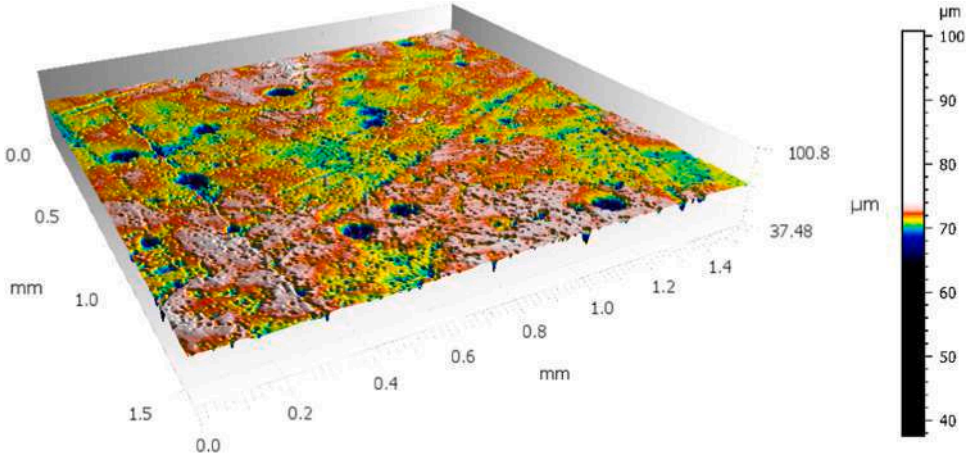

Fig. 6. Raw topography of the PTFE+Pb surface measurement.

Table 1
Topographical characterization results in terms of average (m) and standard deviation (s) of 10 measured locations. SL-Surface parameters.

Parameter	Sa / µm	Sq / µm	Ssk / -	Sku / -	Sp / µm	Sz / µm	Sal / µm	Str / -	Sdq / -
m	0.95	1.47	-2.03	18.35	14.54	37.38	41.65	0.822	0.246
s	0.112	0.160	0.902	7.165	8.344	11.94	4.171	0.1247	0.0286

Table 2
Results of mechanical properties regression. Estimated parameters are reported with estimation uncertainty (95% confidence level, i.e., k = 2).

	E_{IT} / GPa	H_{IT} / MPa
$\hat{a}$	(1.276 ± 0.0620) GPa	(33.15 ± 5.90) MPa
$\hat{b}$	(9.891 ± 0.0320) GPa	(151.8 ± 5.40) MPa
$\hat{c}$ / µm	26.21 ± 0.14	43.46 ± 1.67
$\hat{d}$ / µm	-4.053 ± 0.1050	-11.37 ± 2.063
R^2 coefficient	99.52%	79.07%
RMSE	0.2589 GPa	18.49 MPa

characterization results comparing the average of the characterisation obtained at 10 mN and 7.5 mN. Indentations at 7.5 mN resulted well within the conservative prescription 10% of the layer thickness (2.794 ± 0.438) µm.

Viscoelastic material characterization was addressed according to the experimental design based on dynamic indentation. Fig. 8(b) shows an indentation curve result. Few indentations needed to be eliminated due to poor contact conditions, so an unbalanced design resulted, and a generalized linear model (rather than ANOVA) was required to investigate the systematic effect of material and frequency on the mechanical characterization.

The generalized linear model (GLM), consistently with the main effect plots shown in Fig. 9, indicated, with a risk of error smaller than 5%, that both the material and the frequency of the load application affect the viscoelastic response of the material. In particular, the inclusions of the fine powder of Pb induce a stiffening, i.e. an increase of the Young modulus. The effect of the frequency is also interesting. It has a systematic effect on both the E_{IT} and the storage modulus E', i.e., on the elastic behaviour, regardless of the material, as it can be appreciated from the main effects plot in Fig. 9. Conversely, with a confidence level of 95%, according to the GLM, it does not affect the damping properties, i.e. the loss modulus. Considering the significant effect of the loading frequency, insights are provided by studying the interval plot (error bars at 95% confidence intervals) of the E_{IT} resulting from the quasistatic indentations on the base bulk PTFE and the reinforced PTFE+Pb to estimate the average of the mechanical characterization (see Fig. 10(a)). Similarly, the effect of frequency is highlighted on the PTFE+Pb in Fig. 10(b-c). Increasing the loading frequency results in an apparent stiffening of the material (E' and E_{IT}) because less time is available for the material to elastically recover. Thus, when the next sinusoidal oscillation begins, the extent of the superimposed elastic deformation field is reduced. Viscoelasticity is associated with the molecular rearrangement inside the polymer. If a stress field is applied, parts of the long polymer chains react by changing their position to minimize the stress field. This non-equilibrium asset increases the molecular packing density. When the load is released, the back stress in the material progressively vanishes as the polymer recovers the elastic part of the deformation towards a new equilibrium state [57]. Therefore, as the frequency increases, the indenter tip contacts a surface with a residual compressive stress field from the previous indentation cycle, which locally results in an apparent stiffer response of the material. Fig. 11 provides a schematic depiction of the phenomenon.

3.2.2. Micro-scale characterization

The experimental design described in Section 2.2.2 was implemented, and a resulting indentation result is shown in Fig. 8(c-d). Fig. 12 (a-b) shows the trend of the mechanical characterization in terms of E_{IT} and H_{IT}, respectively. Consistently with the material structure analyzed by optical microscopy (see Fig. 1), a trend of the mechanical characteristics results as a function of the indenter penetration depth. In particular, an increasing trend moving from the PTFE+Pb to the sintered porous bronze is appreciated, with a transition zone. Indeed, the represented results are the effect of the superimposition of the material and the substrate [58]. However, such convolution is sufficient for modelling purposes. Therefore, a nonlinear regression is performed considering, for mathematical purposes of fitting improvement, a logistic growth model:

$$y = a + \frac{b-a}{e^{\frac{h_{c,\max}-c}{d}}} \tag{3.1}$$

with y the dependent variable (either E_{IT} or H_{IT}), and a, b, c and d parameters to be estimated by regression. The results of the model are summarized in Table 2.

Additionally, ECR allows insights into the material response. Fig. 12 (a-b) shows a transition from 10 µm to 50 µm from the material surface.

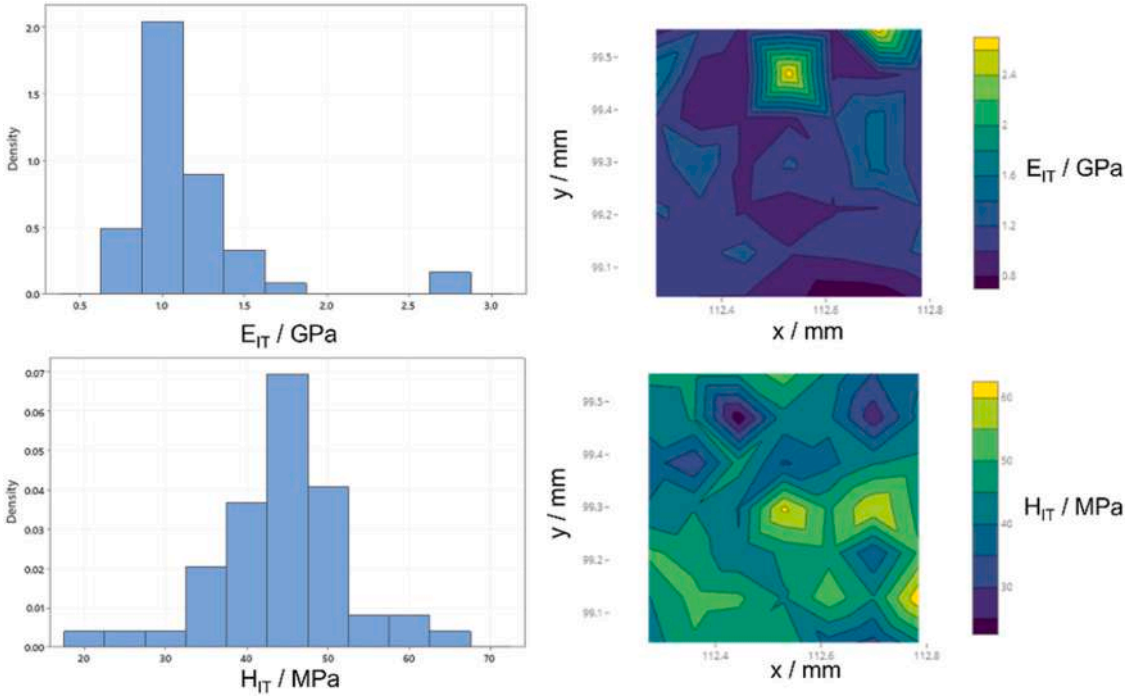

Fig. 7. Histogram and spatial mapping of PTFE+Pb E_{IT} and H_{IT}. Notice the absence of significant deviations from gaussian distribution for the E_{IT}, apart from one outlier, and the more widespread distribution of the H_{IT}.

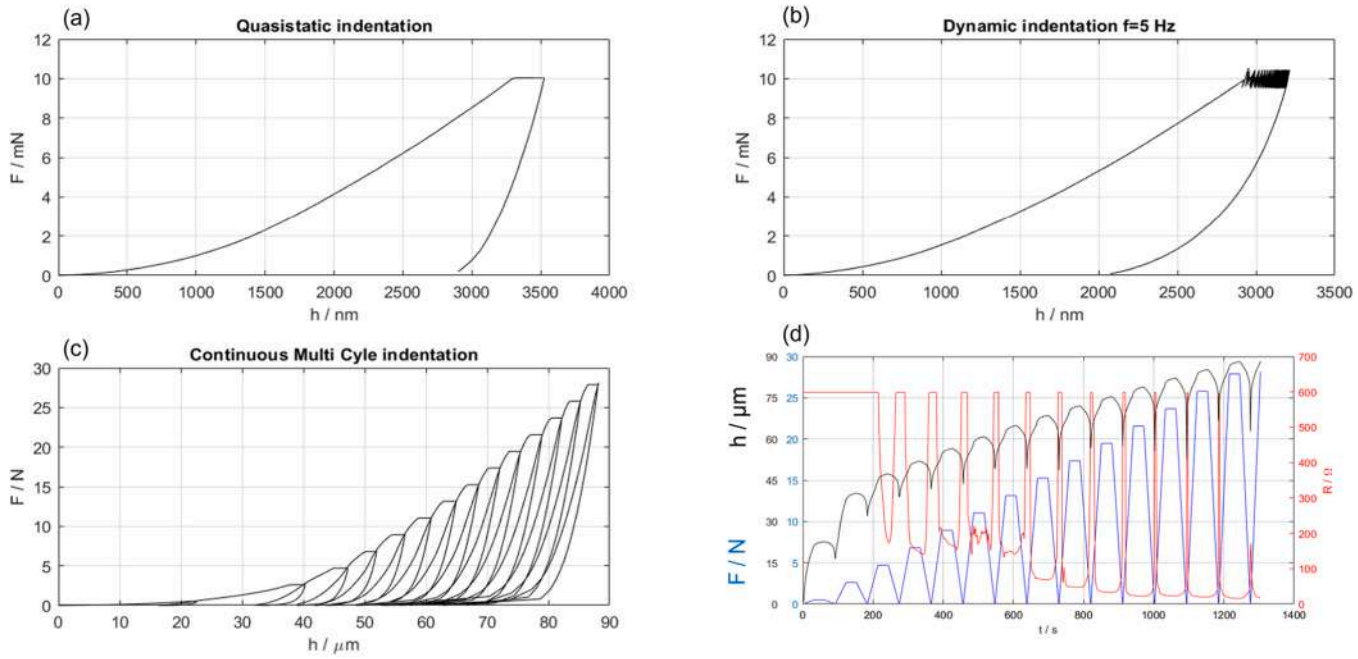

Fig. 8. Results of IIT. Indentation curve of a (a) quasistatic indentation (b) dynamic indentation (notice the sinusoidal load in the holding phase) at 10 mN, and (c) CMC up to 30 N. Measured quantities as a function of time in a CMC indentation (d): black – penetration depth, blue – force and red – resistance. Notice at about 300 s and 20 μm depth a significant disturbance and drop in the resistance indicating contact with bronze.

In-situ resistance measurement shows the presence of a highly insulating material up to 20 μm, i.e. the PTFE+Pb. Then a decrease of the resistance can be seen in Fig. 12(c) up to 50 μm, depth at which a constant value of the electromechanical response indicates the presence of the sintered porous bronze. The transition from the mechanical perspective onsets early due to the mechanical convolution [58]; conversely, the resistance shows a gradient due to the mixed contact with both the PTFE+Pb and the bronze. Consistent results are obtained by analyzing an individual CMC, as in Fig. 8(d). In fact, the resistance trend shows a significant drop and significant disturbances at about 20 μm, indicating an early contact with the substrate. Last, the scatter plot in Fig. 12(c) allows appreciation of the presence of highly insulating material, i.e. PTFE+Pb, even deeper (notice the raw data at 600 Ω for depths larger than 40 μm), which is consistent with the optical analysis indicating pockets of PTFE+Pb in the porous bronze matrix, inherent with the manufacturing procedure of the material.

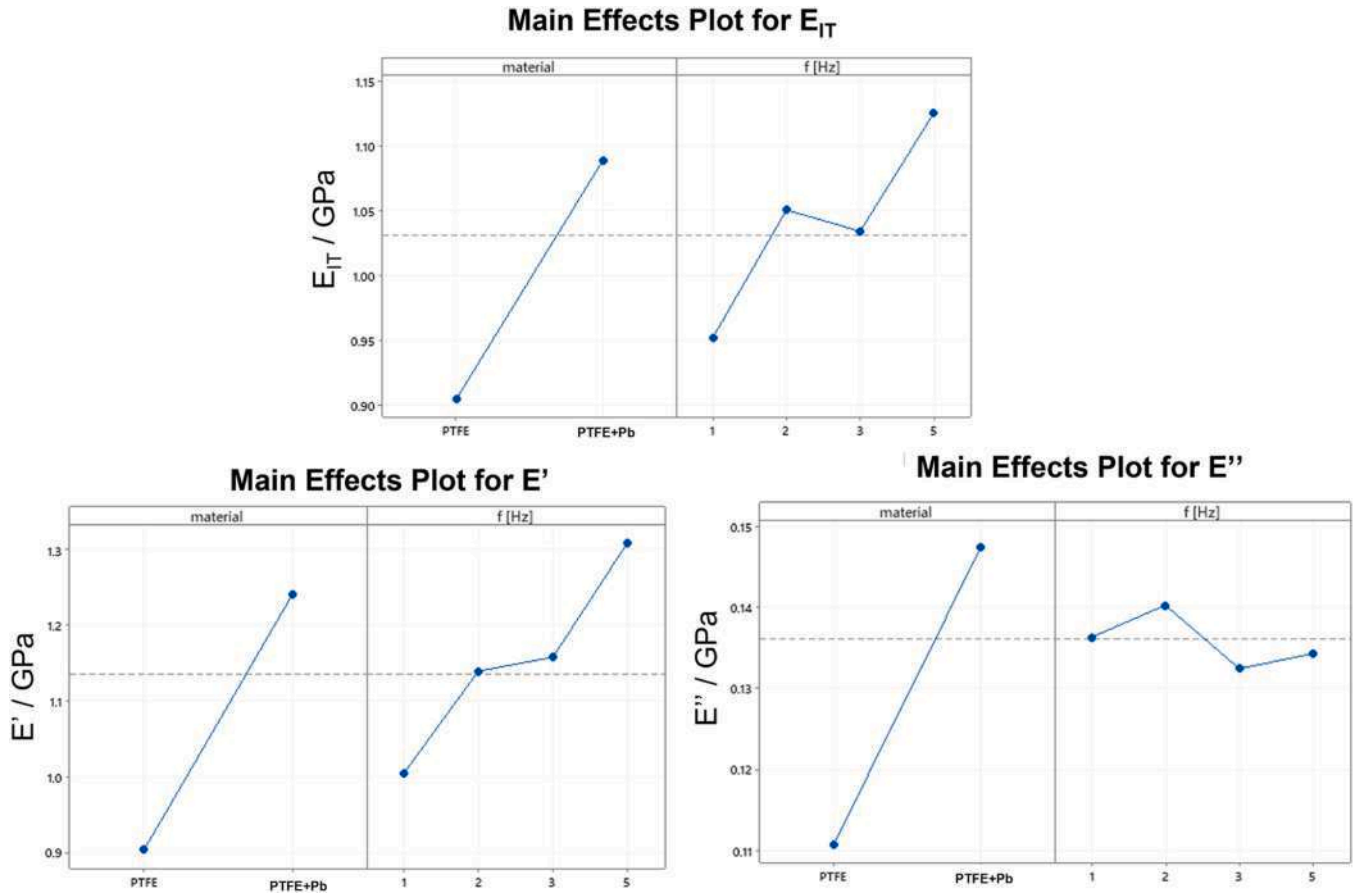

Fig. 9. Main Effects Plots for E_{IT}, the storage modulus E' and the complex component of E_{IT}, i.e., the loss modulus E''. Each point in the graph is the average of the group level identified in the *x*-axis label, mixing all the other factor levels.

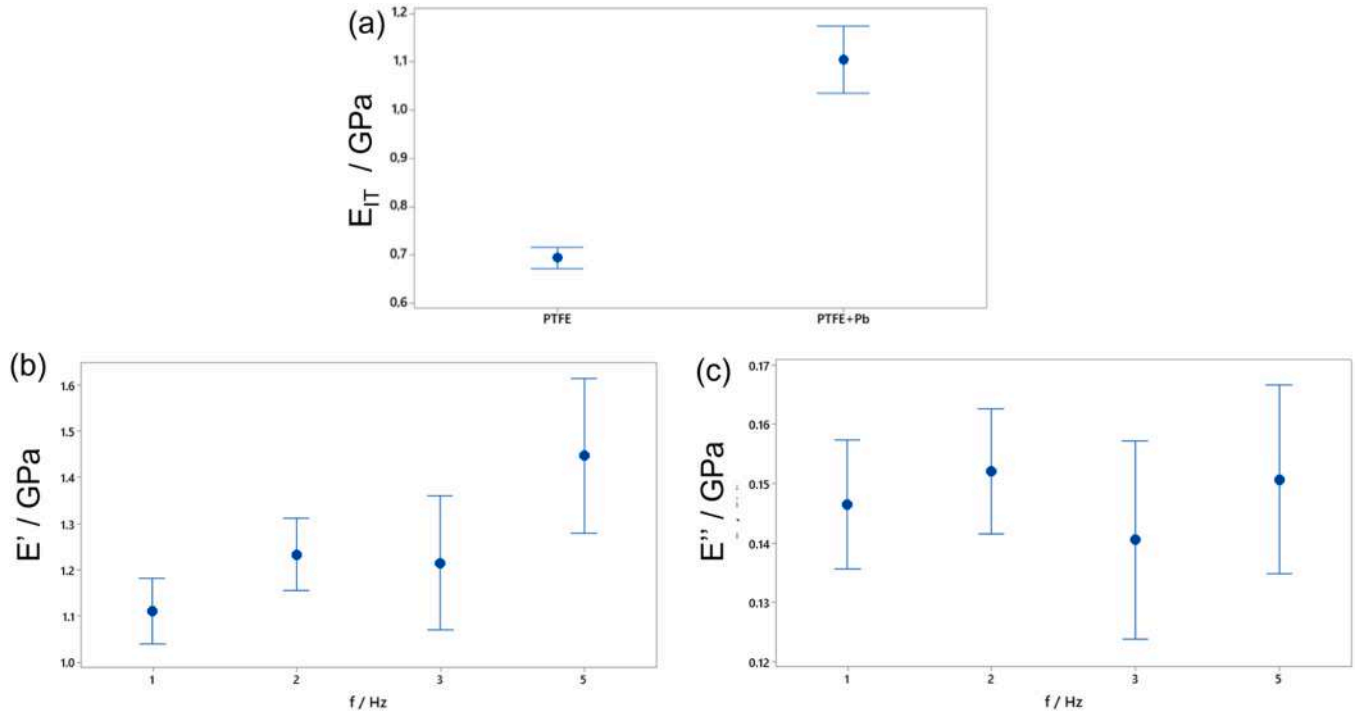

Fig. 10. Interval plot of (a) E_{IT} for the base and the reinforced PTFE with quasistatic indentation (F=10 mN, f=0 Hz). Interval plots showing the effects of frequency on the PTFE+Pb on (b) E' and (c) E''.

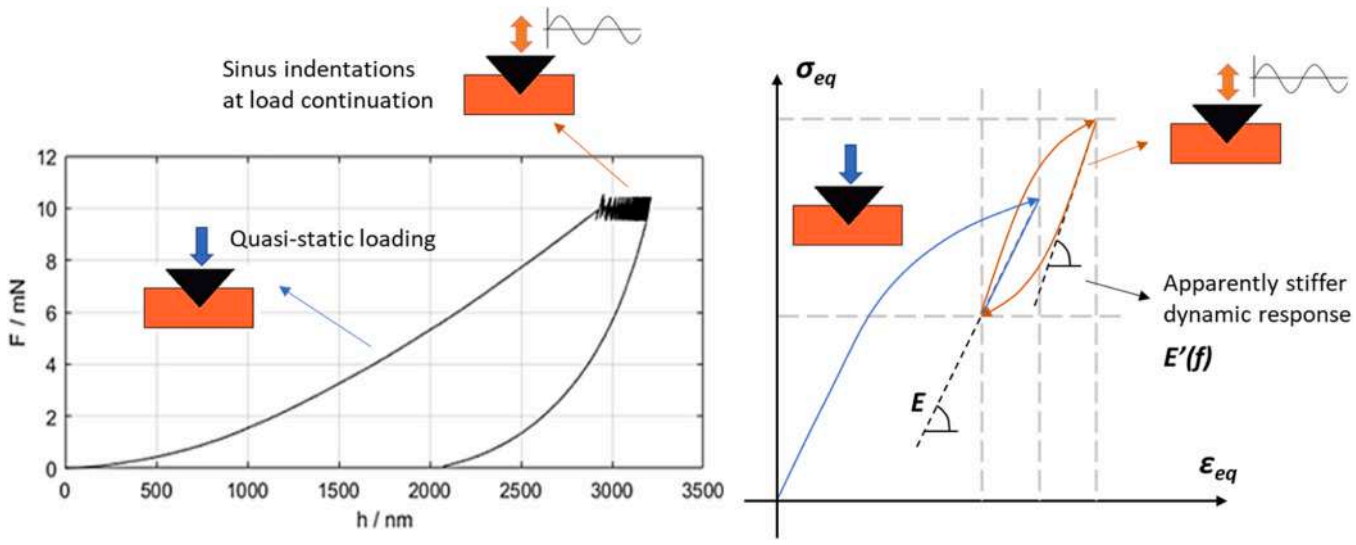

Fig. 11. Apparent dynamic stiffening due to the viscoelastic behavior of the material during the cycling indentation loading at load continuation in IIT tests.

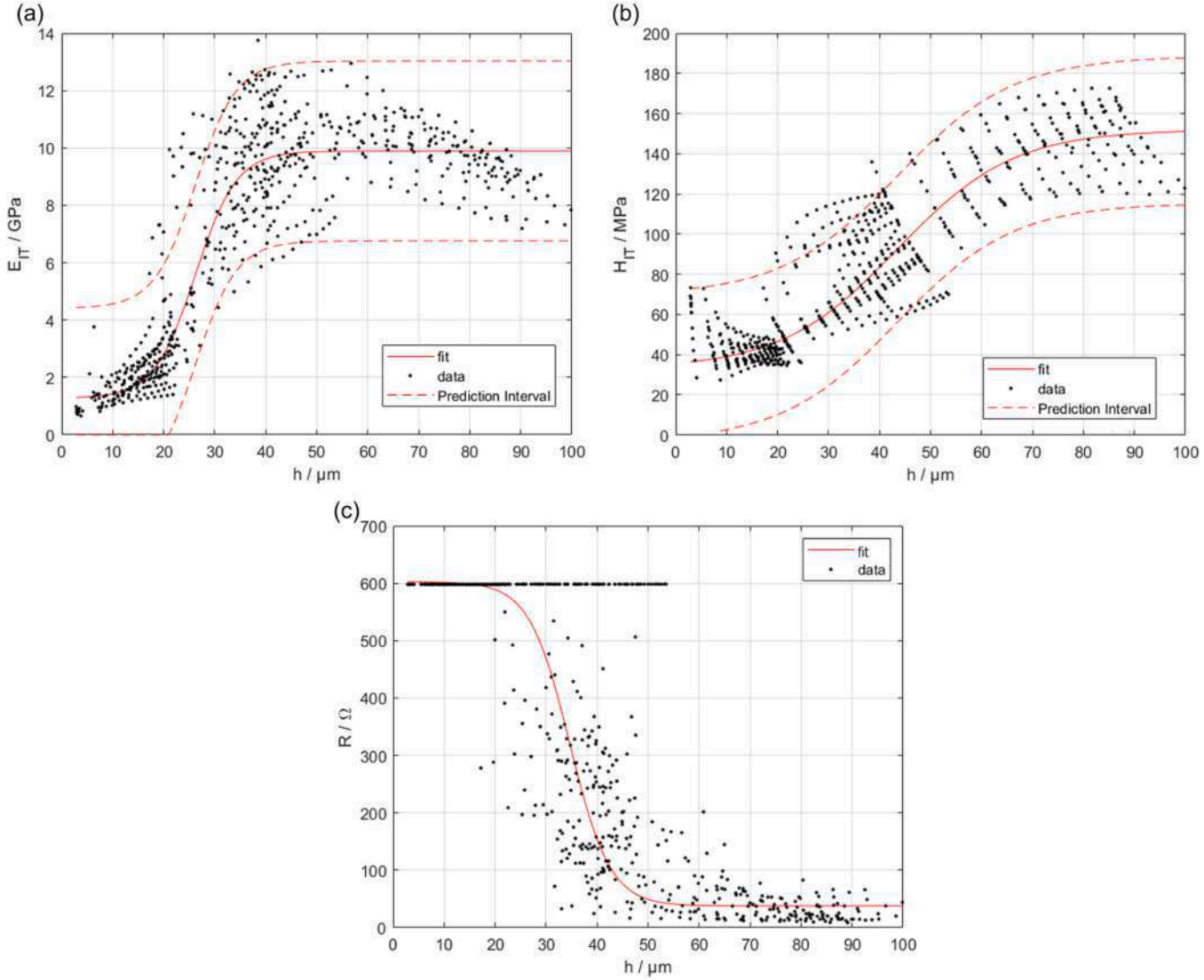

Fig. 12. Results of the micro-scale characterization with augmented CMC indentation. Trend of (a) E_{IT}, (b) H_{IT} and (c) R as a function of the penetration depth. Trend for resistance is only reported to highlight the average behaviour.

3.3. Tribological behaviour

The tribological behaviour of the composite coating is likely dominated by abrasion of the harder steel surface against the softer metal-polymer coating presented. The main results of the pin-on-disk tests are presented in Fig. 13. All the curves shown in the Fig. 13 are the average of the curves obtained from the repetitions of 1900 m sliding tests.

The friction curve presents two stable periods after the initial running-in. Between 50 m and 250 m, the CoF value was equal to about 0.175, while from 400 m up to the end of the test, the value stabilized at about 0.160. The information provided by the online linear wear sensor suggests that these two phases of the test correspond to the wearing-out of the two layers of the composite coating. A slightly higher coefficient of friction is observed as long as the pin remains in contact with the soft outermost PTFE+Pb layer. The transition to a lower stable value was observed at 25 μm of liner wear depth (dashed line in the Fig. 13). This value matches the thickness of the outermost layer measured by optical microscopy (see Fig. 1) and corresponds to a variation of the linear wear trend, as expected by the information provided by the GGB technical sheet. The transition significantly affects also the measurement precision, by yielding larger measurement uncertainties which later stabilises when contact with bronze is fully established, i.e. at linear wear depth larger than 40 μm.

According to the authors, the reason why the CoF was higher in the first part of the test is twofold. The overlay made of the PTFE+Pb polymeric compound is relatively soft and ductile, and at the beginning of the test, it withstands the entire contact load. Despite its high lubricity, when the rigid steel pin slides against it, a large effective contact area is expected due to the ploughing of the hard surface asperities. This effect is further promoted by the rough surface of the pin used in these tests. Moreover, an additional sliding resistance might also be produced by some piling-up effect at the leading edge of the contact due to digging of the pin into the soft layer. When the outermost layer is completely worn-out, the pin reaches the stiffer zone dominated by the porous bronze structure, with a likely decrease in the effective contact area. According to the simplified 2-body abrasive friction model by Rabinowicz [59], the contact area between the ploughing body and the abraded mass, i.e. the section area of the furrow, influences the coefficient of friction. Since ploughing into the bronze-strengthened layer is much more difficult, the CoF would decrease.

Besides, a beneficial third layer rich in PTFE and bronze adhered to the steel surface and filled the roughness furrows and valleys. The presence of such a low conductive layer is proved by the ECR chart, whose value progressively increases after the wear depth exceeds the threshold of the outermost layer. The third layer insulated the coating from direct contact with steel and alleviated the frictional force contributing to the wear rate reduction. The inspection under the optical microscope of the pin (Fig. 14) further supports the hypothesis that high-lubricity stacked layers of compacted debris made of PTFE+Pb and bronze accumulates to the steel counterpart, driving the contact to a regime condition of PTFE+Pb/Bronze-against-PTFE+Pb/Bronze.

Topographical inspection of the worn topographies was performed, resulting in the measurements reported in Fig. 15. For longer tests, besides the deeper track, an increasing amount of galling, i.e. plastically displaced material at the wear track edge, results. Native roughness is negligible with respect to the amount of induced wear, although removed for the estimation of the wear volume by the machine vision methodology [52].

Fig. 16 shows the increasing trend of the effective volume of material lost by the system, according to Eq. (2) [51] that takes into account the contribution of the wear damage (V_w) and galling or plastically displaced material (V_g) as per the ASTM G40 standard definitions. Two wear stages were identified by the diagram, and two corresponding Archard wear rates ($tg\alpha$) were calculated considering the increase in wear volume approximately linear within each stage. The 1st wear stage corresponds to the wearing-out of the outermost soft layer from 0 m to about 300 m. The 2nd stage involves the wearing out of the innermost stiffer layer dominated by the bronze structure. The appearance of the wear track under the optical microscope shown in Fig. 16 supports the fact that the trend variation of the wear volume is actually associated with this layer transition. The corresponding dimensional and dimensionless Archard wear coefficients are listed in Table 3.

4. CONCLUSIONS

This work presented a thorough mechanical and tribological characterization of a metal-polymer composite coating for plain bearings. Although this kind of coatings is widespread in many industrial applications, detailed knowledge of their mechanical properties was lacking

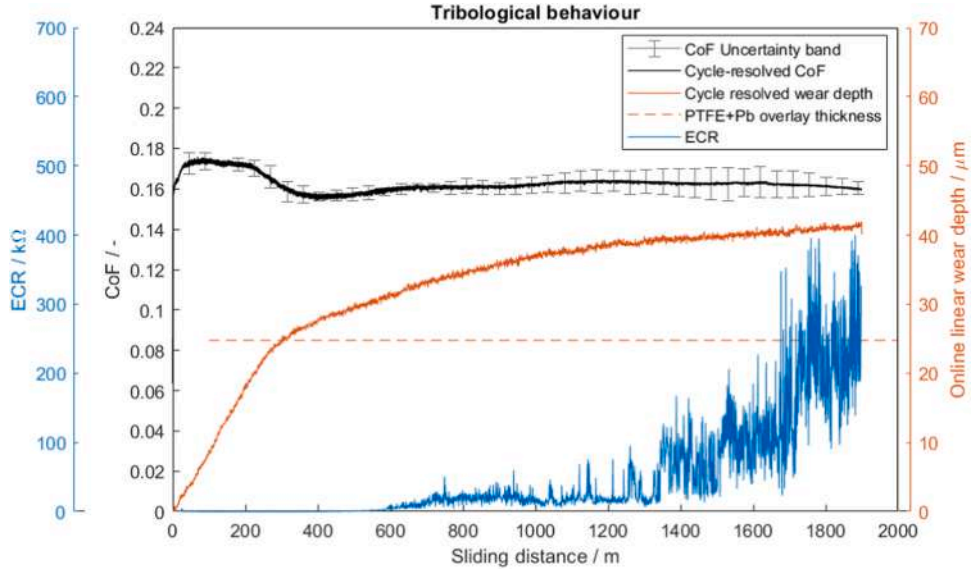

Fig. 13. Tribological behaviour of the PTFE+Pb/Bronze sinter coating against a flat steel pin. The curves are the average of the results obtained with the four repetitions of the linear reciprocating pin-on-disc tests with a duration of 1900 m of sliding. Each point of the friction curve corresponds to the averaging of the absolute CoF values acquired over one single reciprocating cycle. CoF error bars report uncertainty at 95% of the estimated average.

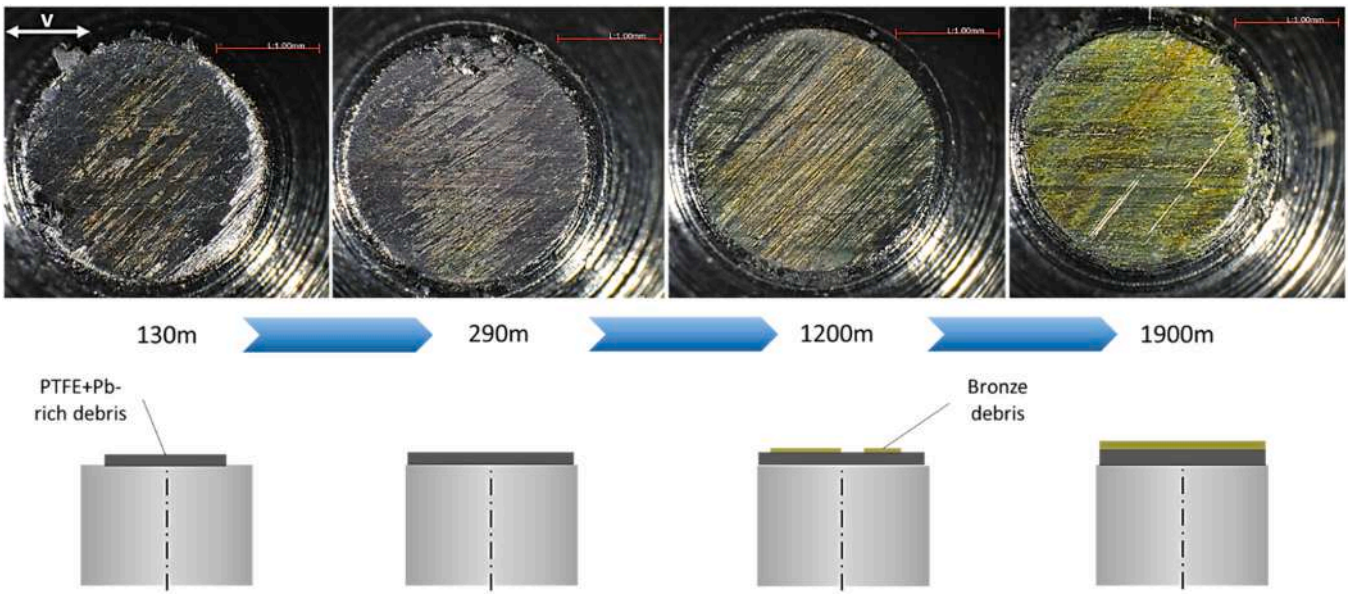

Fig. 14. Growth of a third layer on the pin contact surface during the tests from the initial steel-PTFE+Pb/Bronze interface to an effective PTFE+Pb/Bronze-against-PTFE+Pb/Bronze interface.

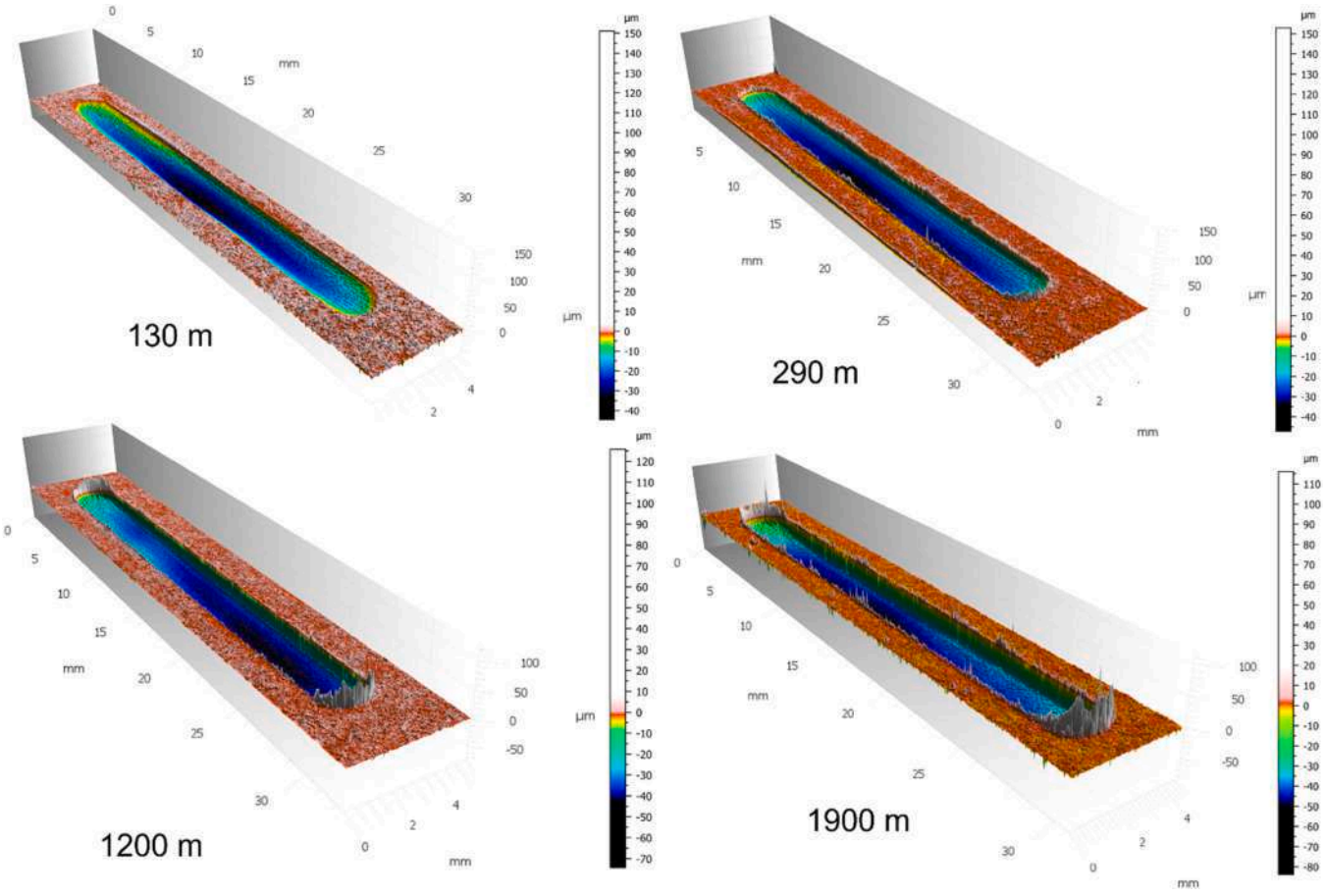

Fig. 15. Measured topographies of pin-on-disc wear tracks. Notice the increase of plastically displaced material for the increasing test lenght.

in the scientific literature. The characterization was carried out by instrumented indentation tests and pin-on-disc tests to measure the evolution of the mechanical and tribological properties along the thickness of the coating. Innovatively, both IIT and pin-on-disc were augmented by in-situ contact resistance measurements to track the contact with the conductive and non-conductive phases of the coating. Despite this complex coating features a highly non-homogeneous structure, the methodology proved effective in characterizing the

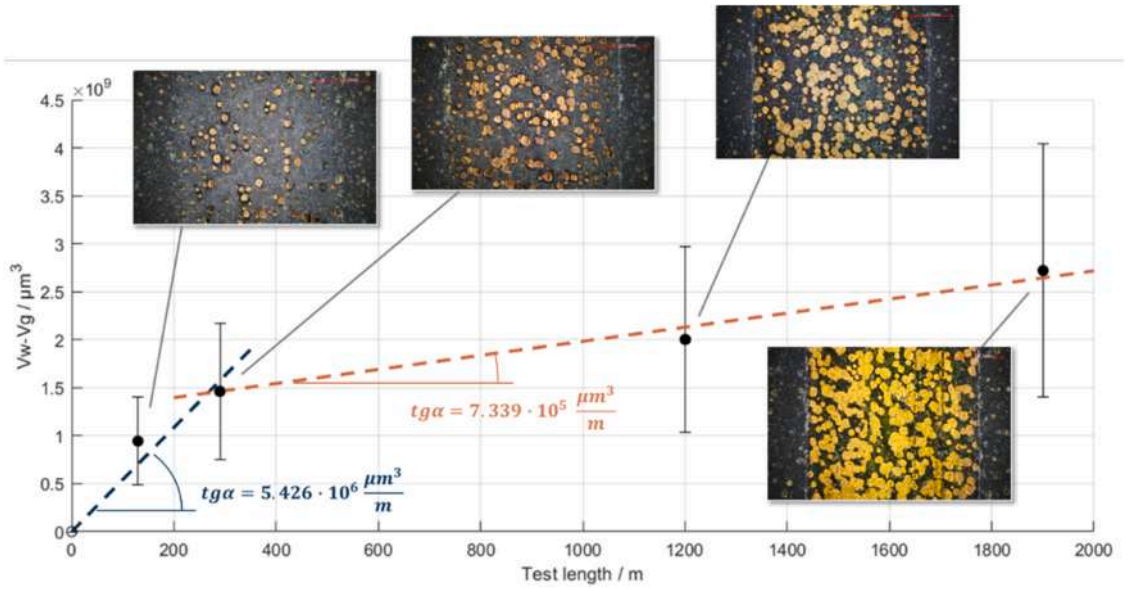

Fig. 16. Evolution of the wear volume and corresponding appearance of the wear track under the optical microscope.

Table 3
Archard wear coefficient of the PTFE+Pb/Bronze coating for Phase I and Phase II.

	Phase I	Phase II
Wear rate / µm^3/m	5.43E+ 06	7.34E+ 05
Dimensional wear coefficient / mm^3/mN	1.09E-04	1.47E-05
Average Hardness / MPa	50	120
Dimensionless wear coefficient / -	5.43E-06	1.76E-06

average properties of the material. The information provided by the data augmentation were essential to substantiate insights on the material mechanical and tribological behaviour and could have been otherwise partially achievable only through destructive cross-sectioning. The mathematical description of the evolution of the material property as a function of depth will allow more accurate numerical modelling of the material behaviour, only roughly approximated in previous literature, but essential in designing its application. This is crucial for applications that involve structural mechanical modelling, including contact mechanics problems or wear modelling during the design or optimization phase. For instance, the optimization of the stress distribution and the wear behaviour at the bushing-rod interface in linear pneumatic actuators is possibly affected by the accurate modelling of the material properties of the bushings, which are often made of this kind of composite coatings. This aspect will be the object of future investigations.

Declaration of Competing Interest

The authors declare that they have no known competing financial interests or personal relationships that could have appeared to influence the work reported in this paper.

Data Availability

Data will be made available on request.

Acknowledgements

The authors would like to thank Mr. C. Lerre for his support in carrying out the experiments and in the preliminary data analysis.This study was carried out within the MICS (Made in Italy – Circular and Sustainable) Extended Partnership and received funding from the European Union Next-GenerationEU (PIANO NAZIONALE DI RIPRESA E RESILIENZA (PNRR) – MISSIONE 4 COMPONENTE 2, INVESTIMENTO 1.3 – D.D. 1551.11-10-2022, PE00000004). This manuscript reflects only the authors' views and opinions, neither the European Union nor the European Commission can be considered responsible for them.

Statement of Originality

The authors state that the work enclosed has not been published previously, that it is not under consideration for publication elsewhere and that its submission is approved by all the authors.

References

[1] Rondinella A, Andreatta F, Turrin D, Fedrizzi L. Degradation mechanisms occurring in PTFE-based coatings employed in food-processing applications. Coatings 2021; 11:1419. https://doi.org/10.3390/coatings11111419.
[2] Natarajan E, Santhosh MS, Markandan K, Sasikumar R, Saravanakumar N, Dilip AA. Mechanical and wear behaviour of PEEK, PTFE and PU: review and experimental study. J Polym Eng 2022;42:407–17.
[3] Rimai DS, DeMejo LP, Mittal KL. Fundamentals of Adhesion and Interfaces. Zeist, The Netherlands: VSP International Science Publisher; 1995.
[4] Straffelini G. Friction and Wear Methodologies for Design and Control. Springer; 2015. https://doi.org/10.1007/978-3-662-48465-4.
[5] Maculotti G, Goti E, Genta G, Mazza L, Galetto M. Uncertainty-based comparison of conventional and surface topography-based methods for wear volume evaluation in pin-on-disc tribological test. Tribol Int 2022;165:107260. https://doi.org/10.1016/j.triboint.2021.107260.
[6] Deli G, Qunji X, Hongli W. Study of the wear of filled polytetrafluoroethylene. Wear 1989;134:283–95. https://doi.org/10.1016/0043-1648(89)90131-2.
[7] Blanchet TA, Kennedy FE. Sliding wear mechanism of polytetrafluoroethylene (PTFE) and PTFE composites. Wear 1992;153:229–43. https://doi.org/10.1016/0043-1648(92)90271-9.
[8] Kowandy C, Richard C, Chen YM. Characterization of wear particles for comprehension of wear mechanisms. Wear 2008;265:1714–9. https://doi.org/10.1016/j.wear.2008.04.036.
[9] Lee J-Y, Lim D-P, Lim D-S. Tribological behavior of PTFE nanocomposite films reinforced with carbon nanoparticles. Compos Part B Eng 2007;38:810–6. https://doi.org/10.1016/j.compositesb.2006.12.006.
[10] Zhang Z-Z, Xue Q-J, Liu W-M, Shen W-C. Friction and wear characteristics of copper and its compound-filled PTFE composites under oil-lubricated conditions. J Appl Polym Sci 1998;70:1455–64. https://doi.org/10.1002/(SICI)1097-4628(19981121)70:8<1455::AID-APP4>3.0.CO;2-6.
[11] Blanchet TA, Kennedy FE, Jayne DT. XPS analysis of the effect of fillers on PTFE transfer film development in sliding contacts. Tribol Trans 1993;36:535–44. https://doi.org/10.1080/10402009308983193.
[12] Conte M, Igartua A. Study of PTFE composites tribological behavior. Wear 2012; 296:568–74. https://doi.org/10.1016/j.wear.2012.08.015.
[13] Khedkar J, Negulescu I, Meletis EI. Sliding wear behavior of PTFE composites. Wear 2002;252:361–9. https://doi.org/10.1016/S0043-1648(01)00859-6.

[14] ggbearings ⟨https://www.ggbearings.com/en/who-we-are/history⟩ (accessed March 23, 2023).
[15] Güngör K, Demirer A. Effects of impregnating PTFE filled with added graphite on wear behavior of sintered bronze plain bearings. Int J Mater Res 2021;112:623–35. https://doi.org/10.1515/ijmr-2020-8067.
[16] S.K.F. Industry. Composite dry sliding bearings – maintenance-free and space-saving. SKF; 1999.
[17] Efimov AI, Semenov AP. Estimating life of metal-fluoroplastic bearings. Russ Eng J 1975;55:3–6.
[18] Belforte G, Raparelli T, Mazza L. Analysis of typical failure situations in pneumatic cylinders under load. Lubr Eng 1992;48:840–5.
[19] Ambu R, Bertetto AM, Mazza L. Re-design of a guide bearing for pneumatic actuators and life tests comparison. Tribol Int 2016;96:317–25. https://doi.org/10.1016/j.triboint.2015.12.043.
[20] Chen J, Zio E, Li J, Zeng Z, Bu C. Accelerated life test for reliability evaluation of pneumatic cylinders. IEEE Access 2018;6:75062–75. https://doi.org/10.1109/ACCESS.2018.2882767.
[21] Manuello Bertetto A, Mazza L, Orrù PF. Contact pressure distribution in guide bearings for pneumatic actuators. Exp Tech 2015;39:46–54. https://doi.org/10.1111/ext.12014.
[22] Fote AA, Wildvank AH, Slade RA. Coefficient of friction of ptfe-impregnated porous bronze versus temperature. Wear 1978;47:255–61. https://doi.org/10.1016/0043-1648(78)90156-4.
[23] Tevrüz T. Tribological behaviours of bronze-filled polytetrafluoroethylene dry journal bearings. Wear 1999;230:61–9. https://doi.org/10.1016/S0043-1648(99)00091-5.
[24] Güngör K, Demirer A. Effects of impregnating PTFE filled with added graphite on wear behavior of sintered bronze plain bearings. Int J Mater Res 2021;112:623–35. https://doi.org/10.1515/ijmr-2020-8067.
[25] Zhang Z-Z, Shen W-C, Liu W-M, Xue Q-J, Li T-S. Tribological properties of polytetrafluoroethylene-based composite in different lubricant media. Wear 1996;196:164–70. https://doi.org/10.1016/0043-1648(95)06892-9.
[26] Ku B, Park Y, Sung C, Han Y, Park J, Hwang Y, et al. Comparison of tribological characteristics between aluminum alloys and polytetrafluoroethylene composites journal bearings under mineral oil lubrication. J Mech Sci Technol 2010;24:1631–5. https://doi.org/10.1007/s12206-010-0508-z.
[27] Kim M.R., Small C.D. The Tribological Performance of Self-Lubricating Bearings Following Secondary Sizing Adjustment. In: Purdue Univertisty, editor. Int. Compress. Eng. Conf., West Lafayette, IN (USA): 2008, p. 1433.
[28] Goti E, Mazza L, Manuello Bertetto A. Wear tests on PTFE+pb linings for linear pneumatic actuator guide bushings. Int J Mech Control 2020;21:155–62.
[29] Leach RK. Characterisation of Areal Surface Texture. Springer, Berlin; 2013. https://doi.org/10.1007/978-3-642-36458-7.
[30] Maculotti G, Feng X, Su R, Galetto M, Leach R. Residual flatness and scale calibration for a point autofocus surface topography measuring instrument. Meas Sci Technol 2019;30. https://doi.org/10.1088/1361-6501/ab188f.
[31] Maculotti G, Genta G, Quagliotti D, Galetto M, Hansen HN. Gaussian process regression-based detection and correction of disturbances in surface topography measurements. Qual Reliab Eng Int 2021:1–18. https://doi.org/10.1002/qre.2980.
[32] ISO 25178–2:2012 Geometrical product specifications (GPS) - Surface texture: Areal. Part 2: Terms, definitions and surface texture parameters. ISO, Genève.
[33] Galetto M, Genta G, Maculotti G. Single-step calibration method for nano indentation testing machines. CIRP Ann 2020;69:429–32. https://doi.org/10.1016/j.cirp.2020.03.015.
[34] Lucca DA, Herrmann K, Klopfstein MJ. Nanoindentation: Measuring methods and applications. CIRP Ann - Manuf Technol 2010;59:803–19. https://doi.org/10.1016/j.cirp.2010.05.009.
[35] Oliver WC, Pharr GM. Measurement of hardness and elastic modulus by instrumented indentation: Advances in understanding and refinements to methodology. J Mater Res 2004;19:3–20. https://doi.org/10.1557/jmr.2004.19.1.3.
[36] ISO 14577–1:2015 Metallic materials-Instrumented indentation test for hardness and materials parameters - Part 1: Test method. ISO, Genève.
[37] Settineri L, Levi R. Surface properties and performance of multilayer coated tools in turning inconel. CIRP Ann - Manuf Technol 2005;54:515–8. https://doi.org/10.1016/S0007-8506(07)60158-9.
[38] Maculotti G, Senin N, Oyelola O, Galetto M, Clare A, Leach R. Multi-sensor data fusion for the characterisation of laser cladded cermet coatings. Eur Soc Precis Eng Nanotechnol, Conf Proc - 19th Int Conf Exhib EUSPEN 2019;2019:260–3.
[39] Maculotti G, Genta G, Lorusso M, Galetto M. Assessment of heat treatment effect on AlSi10Mg by selective laser melting through indentation testing. KEM 2019;vol. 813. https://doi.org/10.4028/www.scientific.net/KEM.813.171.
[40] Maculotti G., Genta G., Carbonatto A., Galetto M. Uncertainty-based comparison of the effect of the area shape function on material characterisation in nanoindentation testing. Proc. 22nd Int. Conf. Exhib. EUSPEN, Genève: 2022.
[41] Maculotti G., Genta G., Galetto M. Criticalities of iterative calibration procedures for indentation testing machines in the nano-range. Proc. 20th Int. Conf. Exhib. EUSPEN, Genève: Euspen; 2020, p. 2–5.
[42] Kholkhujaev J, Maculotti G, Genta G, Galetto M. Calibration of machine platform nonlinearity in Instrumented Indentation Test in the macro range. Precis Eng 2023;81:145–57. https://doi.org/10.1016/j.precisioneng.2023.02.005.
[43] Yunus EM, McBride JW, Spearing SM. The relationship between contact resistance and contact force on Au-coated carbon nanotube surfaces under low force conditions. IEEE Trans Compon Packag Technol 2009;32:650–7. https://doi.org/10.1109/TCAPT.2009.2014964.
[44] Pharr G, Oliver WC, Cook RF, Kirchner PD, Kroll MC, Dinger TR, et al. Electrical resistance of metallic contacts on silicon and germanium during indentation. J Mater Res 1992;7:961–72. https://doi.org/10.1557/JMR.1992.0961.
[45] Greenwood JA. Constriction resistance and the real area of contact. Br J Appl Phys 1966;17:1621–32. https://doi.org/10.1088/0508-3443/17/12/310.
[46] Sprouster DJ, Ruffell S, Bradby JE, Stauffer DD, Major RC, Warren OL, et al. Quantitative electromechanical characterization of materials using conductive ceramic tips. Acta Mater 2014;71:153–63. https://doi.org/10.1016/j.actamat.2014.02.028.
[47] Herbert EG, Oliver WC, Pharr GM. Nanoindentation and the dynamic characterization of viscoelastic solids. J Phys D Appl Phys 2008;41:74021. https://doi.org/10.1088/0022-3727/41/7/074021.
[48] Hay J, Crawford B. Measuring substrate-independent modulus of thin films. J Mater Res 2011;26:727–38. https://doi.org/10.1557/jmr.2011.8.
[49] Hay J, Crawford B. Measuring substrate-independent modulus of thin films. J Mater Res 2011;26:727–38. https://doi.org/10.1557/jmr.2011.8.
[50] ASTM G40–17 Standard Terminology Relating to Wear and Erosion.
[51] Leite MV, Figueroa CA, Gallo SC, Rovani AC, Basso RLO, Mei PR, et al. Wear mechanisms and microstructure of pulsed plasma nitrided AISI H13 tool steel. Wear 2010;269:466–72. https://doi.org/10.1016/j.wear.2010.04.037.
[52] Genta G, Maculotti G. Uncertainty evaluation of small wear measurements on complex technological surfaces by machine vision-aided topographical methods. CIRP Ann - Manuf Technol 2021;70.
[53] Maculotti G, Goti E, Genta G, Mazza L, Galetto M. Uncertainty-based comparison of conventional and surface topography-based methods for wear volume evaluation in pin-on-disc tribological test. Tribol Int 2022;165:107260. https://doi.org/10.1016/j.triboint.2021.107260.
[54] Maculotti G., Goti E., Genta G., Marchiandi G., Mura A., Mazza L., et al. Effect of track geometry on the measurement uncertainty of wear in pin-on-disc tribological test. Proc 21st Int Conf Exhib EUSPEN 2021.
[55] Maculotti G, Pistone G, Vicario G. Inference on errors in industrial parts: Kriging and variogram versus geometrical product specifications standard. Appl Stoch Model Bus Ind 2021;37:839–58. https://doi.org/10.1002/asmb.2603.
[56] ISO 14577–4:2015 Metallic materials - Instrumented indentation test for hardness and materials parameters - Part 4: Test method for metallic and non-metallic coatings. ISO, Genève.
[57] McCrum NG, Buckley CP, Buckley CP, Bucknall CB. Principles of polymer engineering. Oxford University Press (USA),; 1997.
[58] Puchi-Cabrera ES, Staia MH, Iost A. Modeling the composite hardness of multilayer coated systems. Thin Solid Films 2015;578:53–62. https://doi.org/10.1016/j.tsf.2015.01.070.
[59] Rabinowicz E. Friction and Wear of Materials. 2nd Editio. New York: John Wiley & Sons; 1995.